26 May 2010, 4:45 pm - 6:45 pm

Design of Bridges Against Seismic Faulting : Methodology and Applications

Ioannis Anastasopoulos
National Technical University of Athens, Greece

Takis Georgarakos
National Technical University of Athens, Greece

Rallis Kourkoulis
National Technical University of Athens, Greece

George Gazetas
National Technical University of Athens, Greece


Fifth International Conference on
Recent Advances in Geotechnical Earthquake Engineering and Soil Dynamics
and Symposium in Honor of Professor I.M. Idriss
May 24-29, 2010 • San Diego, California

DESIGN OF BRIDGES AGAINST SEISMIC FAULTING : METHODOLOGY AND APPLICATIONS

Ioannis Anastasopoulos
Nat. Technical Univ. Athens
15780, Athens, Greece

Takis Georgarakos
Nat. Technical Univ. Athens
15780, Athens, Greece

Rallis Kourkoulis
Nat. Technical Univ. Athens
15780, Athens, Greece

George Gazetas
Nat. Technical Univ. Athens
15780, Athens, Greece

ABSTRACT

This paper presents a methodology for design of bridge–foundation systems against seismic faulting. The problem is decoupled in two steps. Step 1 deals with the response of a single bridge pier and its foundation subjected to faulting–induced deformation ; Step 2 deals with the detailed model of the superstructure, which is subjected to differential displacements computed in Step 1. We analyze typical viaduct and underpass bridges, founded on piles or caisson foundations. Piled foundations are found to be vulnerable to faulting–induced deformation. While end–bearing piles cannot really sustain any appreciable bedrock offset, floating piles may perform better, especially if combined with hinged pile–to–cap connections. Statically–determinate superstructures are shown to be less sensitive to faulting– induced differential displacements and rotations. Finally, an application of the method is shown for a major bridge, demonstrating the feasibility of design against seismic faulting.

.

INTRODUCTION

In a large magnitude earthquake, structures on top of a fault outcrop may undergo significant differential movements that could lead to failure. Seismic codes have thus prohibited construction in the "immediate vicinity" of seismically active faults. But for long facilities and structures such as water channels, tunnels, pipelines, embankments, and long bridges crossing several geologic formations, such a prohibition has often been impossible to respect. Moreover, past and recent earthquakes have revealed that survival of structures "on top of a fault" is not impossible — even when fault displacements are large (of the order of meters).

In fact, the three 1999 earthquakes in Turkey (Kocaeli and Düzce-Bolu) and Taiwan (Chi-Chi), provided many examples of satisfactory structural performance [Youd et al., 2000; Erdik, 2001; Bray, 2001; Ulusay et al., 2002], serving as an actual confirmation of the older belief that structures can be designed against large tectonic displacements [Duncan & Lefebvre, 1973; Youd, 1989; Berrill, 1983].

Nevertheless, several bridges were damaged due to surface faulting in the 1999 Chi-Chi earthquake [Kawashima, 2001; Pamuk et al., 2005]. One such example is illustrated in Fig. 1, referring to a prestressed concrete bridge, the Bei-Fung viaduct in Fung-Yan City [photos adapted from Hwang, 2000]. The Chelungpu thrust fault crossed its south abutment with an upthrust of about 7 m. The result: collapse of two spans of the bridge due to differential displacement between the piers.

Bridge failures, but also successes, were also reported after the 1999 Turkey earthquakes [Ulusay et al., 2002; Pamuk et al., 2005]. One such case is the failure of the 100 m Arifiye Overpass, near Adapazari. Consisting of four simply supported pre-stressed concrete spans, it was crossed by the 2 m offsetting fault: all spans fell off due to unseating.

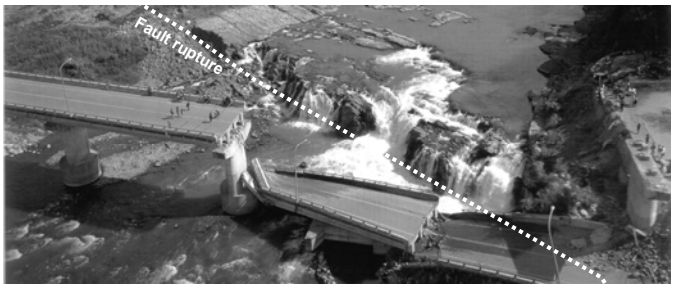

Fig. 1. Collapse of two spans of the Bei-Fung bridge due to tectonic dislocation in the 1999 Chi-Chi (Taiwan) earthquake.

Evidently, such failures are the result of a seismic design which did not systematically study the consequences of fault imposed deformations. To bridge the apparent gap in our understanding, recent research efforts combining field studies, centrifuge model testing, and numerical modeling [Anastasopoulos & Gazetas 2007; Bransby et al. 2008 ; Faccioli et al. 2008 ; Anastasopoulos et al. 2007; 2009] have culminated in the development of a validated methodology for analysis and design of foundation–structure systems against surface fault rupture. It was shown that foundation continuity and stiffness are critical for the survival of buildings.

However, for bridges such continuity is meaningless: bridges are founded on separate supports. While a building on a continuous and stiff foundation may "convert" the imposed dislocation to rigid-body rotation without being substantially distressed, a bridge cannot avoid the differential displacement between its supports (piers). As attested by the previously discussed case histories, such differential displacement may cause structural failure or deck fall, depending on the type of the superstructure.

The basic goal of this paper is to develop a fundamental methodology for bridge design against large tectonic deformation. Since this work was part of a research project in Greece, emphasis is placed on normal faulting (the dominant mode in Greece).

METHODOLOGY

The problem investigated herein and the employed analysis methodology is illustrated in Fig. 2. The analysis of the bridge–foundation system is conducted in two steps, in which the interaction between rupture, soil, foundation, and superstructure is rationally taken into account.

In Step 1 (local level), we analyze the response of a single bridge pier subjected to fault rupture deformation. A detailed model is employed for the aforementioned fault rupture soil–foundation–structure interaction (FR-SFSI), with the superstructure modeled in a simplified manner: the pier, of height H_p and stiffness EI_p , is included in the model; the bridge deck is replaced by equivalent lateral and rotational springs, K_x and K_θ, respectively. For the case of a continuous deck monolithically connected to piers, K_x represents the axial stiffness of the deck and K_θ the bending stiffness of the pier-deck connection. Correspondingly, for a seismically isolated bridge, K_x and K_θ represent the lateral and rotational stiffness of the (elastomeric) bearings. The output of this step is dual: (i) it provides information regarding the distress of the foundation system ; (ii) it provides the necessary input for the second step: horizontal and vertical displacements Δx and Δy and the rotation θ at the base of the pier.

In Step 2 (global level), the detailed model of the superstructure is subjected to the computed Δx , Δy , and θ from Step 1.

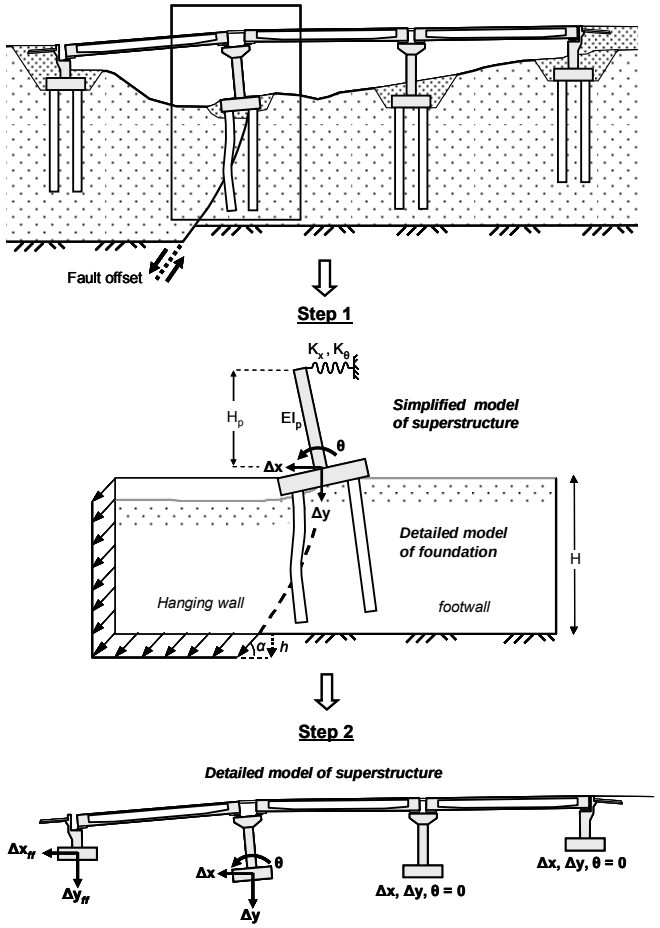

Fig. 2. Methodology : analysis of the soil–structure system is conducted in two steps. In Step 1, we analyze the response of a single bridge pier ; in Step 2, the detailed model of the superstructure is subjected to the computed displacements and rotations of Step 1.

Bridge systems were categorized according to their geometric characteristics, the typology of their superstructure, and their foundation. Based on this, and aiming to render the results of this research as general as possible, two generalized bridge types were selected : (i) a typical 350 m long viaduct bridge (Figure 3), and (ii) a typical 75 m long 3-span overpass bridge (Figure 4). For each bridge type, alternative superstructure typologies were investigated.

As shown in Fig. 3, five different alternatives were investigated for the typical viaduct :

(i) a 7-span viaduct, with continuous deck monolithically connected to piers ;
(ii) the same system, but the deck supported through elastomeric bearings ; and
(iii) 7 simply supported decks on elastomeric bearings.

The deck is a box section of sectional stiffness EI_d = 100 GNm^2, adequate for standard construction of the 50 m spans.

The sectional stiffness EI_p of the piers varies with their height H_p, so that the member stiffness of each pier K_p is kept constant : a commonly used rule in practice. The value of K_p was computed based on the mass of the deck m_d , so that the dominant period T of each system corresponds to realistic values : T = 1.0 sec for alternative (a) ; T = 1.5 sec for alternative (b). For the seismically isolated alternatives (b and c), the stiffness of the elastomeric bearings was computed so that T = 3.0 sec.

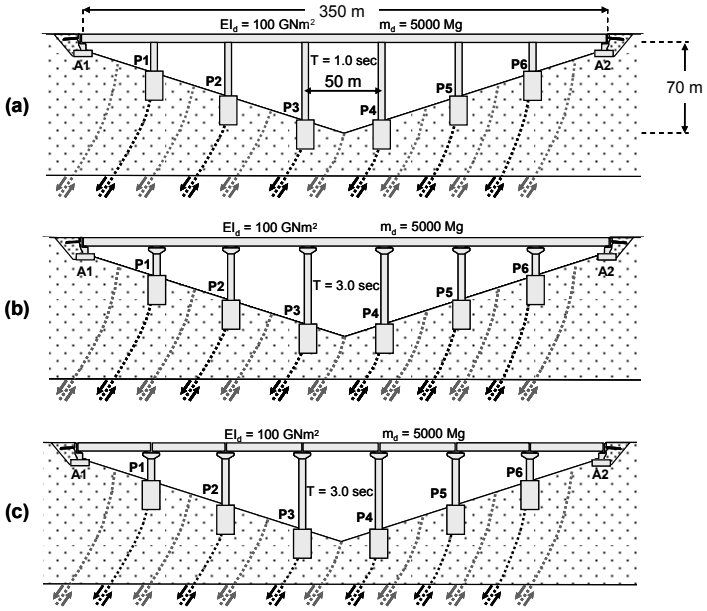

Fig. 3. Parametrically investigated viaducts : (a) continuous deck monolithically connected to piers ; (b) same system, but deck supported through elastomeric bearings ; (c) 7 simply supported spans on elastomeric bearings.

Two alternatives were selected for the typical overpass bridge (Fig. 4) :

(i) a three-span continuous deck monolithically connected to piers; and
(ii) three simply supported decks on elastomeric bearings.

As in the previous case, the two alternatives were selected to correspond to realistic bridges. Since the span is smaller (25 m), a smaller box section of EI_d = 60 GNm2 was selected. The cross-sectional stiffness of piers was set to EI_p = 20 GNm^2, so that (for m_d = 800 Mg) the non-isolated system would yield T = 0.5 sec in the longitudinal direction (a typical value). For both alternatives, the stiffness of the elastomeric bearings was selected so as to achieve T = 2.5 sec.

As depicted in Figs. 3 and 4, for each bridge type different scenarios were investigated with respect to the location of fault outcropping : the first set (in grey) assumes fault rupture emergence between two consecutive piers; the second (in black) refers to the case of the dislocation taking place at the location of a pier. In the first case, the input to the detailed bridge model (of Step 2) only includes the displacements Δx and Δy, and the interaction analysis of Step 1 is redundant. In the second case (rupturing at the location of a pier), the FR–SFSI analysis is mandatory to compute Δx and Δy (which are affected substantially by the presence of the pier foundation), and the input to the Step 2 model also includes the rotation θ at the base of the pier, which is equally (if not even more) important to Δx and Δy, especially for the case of tall piers. At the foundation level, an adequate number of local rupture location scenarios were parametrically investigated. For the input to the subsequent bridge superstructure analysis (Step 2), the worst-case local rupture location scenario was employed.

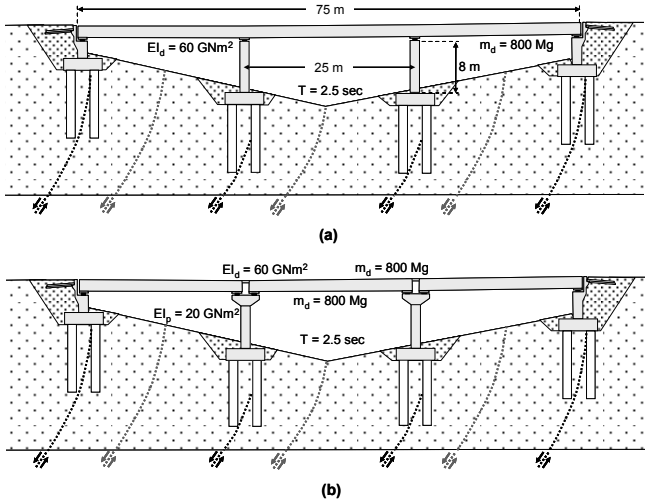

Fig. 4. Parametrically investigated overpass bridges : (a) continuous deck supported on elastomeric bearings ; (b) 3 simply supported spans on elastomeric bearings.

Since the response of the bridge system largely depends on the response of its foundation to the imposed tectonic dislocation, a number of typical foundation systems were parametrically investigated in the first analysis step. As for the superstructure, realistic foundation systems were selected for analysis, corresponding to the parametrically analyzed bridge types (Figures 3 and 4). The idealized foundation types of Fig. 5 were selected for analysis :

(a) a "small" 2 × 4, d = 1.0 m, L = 15 m pile group, suitable for the overpass bridge ;
(b) a "large" 3 × 3, d = 1.5 m, L = 15 m pile group, suitable for the 7-span viaduct bridge ;
(c) a 10 m× 10 m × 15 m caisson foundation, also suitable for the 7-span viaduct (for poor soil conditions).

In all cases, different scenarios were investigated with respect to the soil conditions, with Layer 1 ranging from idealized loose to dense sand [Anastasopoulos et al., 2007], and Layer 2 (for the piled foundations) ranging from dense sand to rock-type material. Thus, both floating (with Layer 2 being the same with Layer 1) and end-bearing piles (with Layer 2 being substantially stiffer than Layer 1) were investigated.

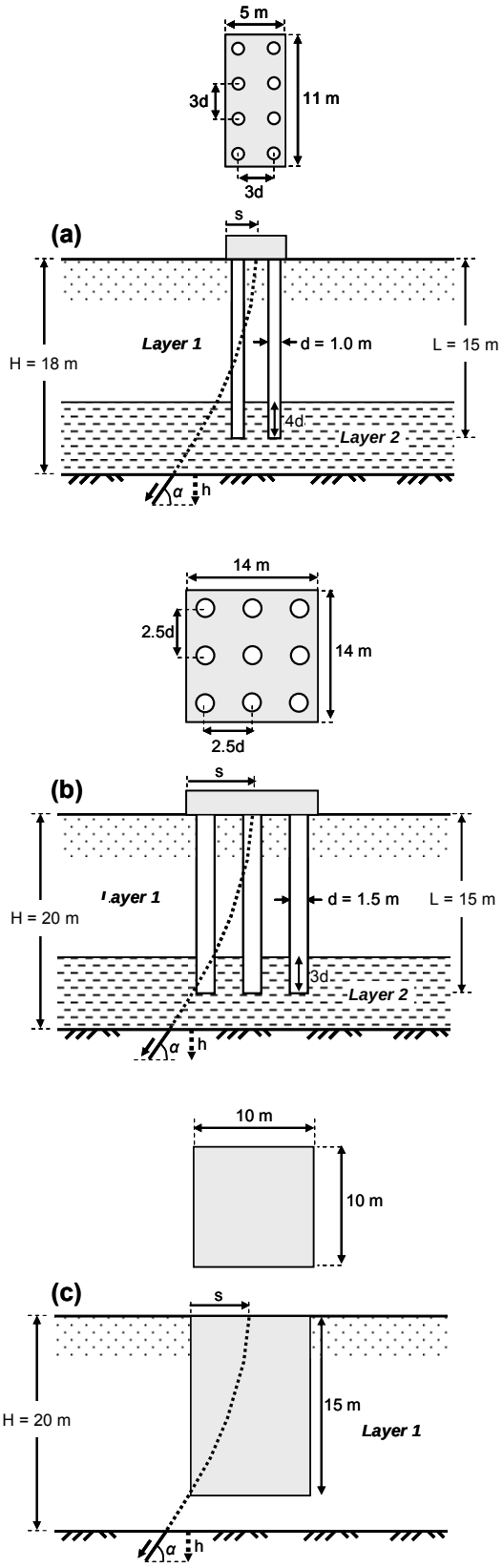

Fig. 5. Parametrically investigated foundation systems : (a) 2 x 4, d = 1.0 m, L = 15 m pile group ; (b) 3 x 3, d = 1.5 m, L = 15 m pile group ; and (c) 10 m x 10 m x 15 m caisson.

The following section discusses the finite element (FE) analysis method employed for FR–SFSI analysis at the local pier-foundation level (Step 1). Then, the key findings concerning the response of piled and caisson foundations are discussed, followed by the main results of the global analysis of the superstructure (Step 2).

NUMERICAL ANALYSIS METHOD

The analysis is conducted in 3-D, utilizing the FE code ABAQUS. The soil is modeled with hexahedral (8-node) brick-type elements of dimension d_{FE} = 1 m to achieve a reasonably refined mesh, as documented in detail in Anastasopoulos et al. [2007]. In the case of caisson foundations, the mesh is made sparser far from the area of interest. The caisson is also modeled with brick-type elements, assumed linear elastic : E = 25 GPa (concrete). Following the results of an initial sensitivity study, the total width of the model was set to B = 3H. Although this is less than the B = 4H recommendation of Bray [1990; 1994a; 1994b], the sensitivity analysis showed that the results of interest are hardly affected, while the computational time was reduced substantially. Hence, it was accepted as a reasonable compromise.

The superstructure is taken into account, as described previously : the pier is modeled with beam elements ; the deck with appropriate grounded springs. In all cases, half of the foundation system is analyzed, taking advantage of problem symmetry.

In the case of piled foundations, the mesh is refined further close at the area of the piles ($d_{FE} \approx$ 0.25 m) to capture their geometry. "Dummy" (i.e. of zero mass and stiffness) brick-type elements are used to model the geometry of the piles. The piles are actually modeled with beam elements, rigidly connected to the peripheral nodes of the corresponding dummy elements. This way, soil-to-pile interaction is modeled realistically : contact is attained on the actual periphery of the pile and the actual pile tip area. The piles are connected to a rigid pile cap, which is modeled with hexahedral brick-type elements. Both the piles and the pile cap are assumed liner elastic, with E = 25 GPa (concrete).

The analysis is performed in two steps. First, fault rupture propagation through soil is analyzed in the free field, ignoring the presence of the foundation (pile group or caisson). Then, knowing the location of fault rupture emergence, the foundation is positioned so that the unperturbed rupture outcrops at distance s from its hanging wall (left) edge. In the case of the "small" 2 × 4 pile group, five scenarios were parametrically investigated with respect to the location of fault outcropping : s = 2, 5, 7, 8, 9, 10, and 11 m. Observe that although the width of the pile-cap is 5 m, due to the non-vertical propagation of the rupture larger values of s are required to cross the pile group at all possible locations. Similarly, for the "large" 3 × 3 pile group, s = 3, 7, 11, 15, 16, and 20 m ; and for the caisson, s = 1, 5, 9, 13, 14, and 18 m.

CONSTITUTIVE MODELING OF SOIL

Soil behavior is modeled with an elastoplastic constitutive model with a Mohr-Coulomb failure criterion and isotropic strain softening, encoded in ABAQUS through a user subroutine. Strain softening is introduced by reducing the mobilised friction angle φ_{mob} and the mobilised dilation angle ψ_{mob} with the increase of plastic octahedral shear strain. Soil behaviour before yielding is modeled as linear elastic. Model parameters are calibrated through direct shear test results, and an approximate scaling method is employed to take account of scale effects. Two idealized soil materials and a simplified rock-type material are utilized in the analysis :

- Loose Sand : $\varphi_p = 32^o$, $\varphi_{res} = 30^o$, $\psi_p = 3^o$, $\gamma_y = 0.030$.
- Dense Sand : $\varphi_p = 45^o$, $\varphi_{res} = 30^o$, $\psi_p = 18^o$, $\gamma_y = 0.015$
- Rock-type : $\varphi_p = 37^o$, $\varphi_{res} = 25^o$, $\psi_p = 15^o$, $\gamma_y = 0.002$.

where : γ_y is a parameter associated with the initial "elastic" response of the soil material, the plastic shear strain at peak conditions, φ_{res} the residual value of the friction angle, and ψ_p the ultimate dilation angle.

The FE modeling methodology employed herein has been extensively validated through qualitative comparisons with numerous published experimental data [Cole & Lade, 1984] and earlier case histories [Slemmons, 1957; Brune & Allen, 1967; Taylor et al., 1985], semi-quantitative comparisons with case histories from the 1999 earthquakes of Kocaeli and Turkey [Anastasopoulos & Gazetas, 2007; Faccioli et al., 2008], and – most importantly – through quantitative blind predictions of centrifuge model tests [Anastasopoulos et al. 2009].

PILE GROUPS

Pile foundations are traditionally used to protect the superstructure by minimizing the settlements and the dynamic (shaking-induced) rotations. However, their performance to concentrated deformation is not always beneficial. Evidence from recent earthquakes has implicated the piles for the observed structural damage. The previously discussed failure of several piles of the Bolu Viaduct in the second 1999 Turkey earthquake is definitely one such case. Another such example is the damage of the pile-supported Attatürk Stadium in Denizerler during the earlier 1999 Kocaeli earthquake.

This section discusses the key findings of the parametric analysis at the local foundation level for the case of piled foundations. The detailed presentation of all analysis results is out of the scope of this paper. Hence, we focus on characteristic results that provide insight to the governing interaction mechanisms.

Performance of "small" 2 x 4 pile-group

We first discuss the performance of the "small" 2× 4 pile group, which is adequate for the typical overpass bridge. Layer 1 is assumed to be the idealized dense sand and Layer 2 the idealized rock-type material — the case of end-bearing piles. The vertical superstructure load transmitted onto the group is equal to V = 2500 kN, typical of an overpass bridge. The role of the superstructure is modeled in a simplified manner, as illustrated in Fig. 2.

Fig. 6 depicts the response of the pile group subjected to h = 0.05 m normal faulting at distance s = 5, 7, 8, and 10 m, in the form of FE deformed mesh with superimposed plastic strain. The selection of such a small imposed bedrock dislocation is deliberate: to demonstrate clearly the sensitivity of pile foundations to this type of loading. As seen in Fig. 6a, for s = 5 m (i.e. the unperturbed fault rupture would outcrop near the right edge of the pilecap), the pile group "forces" the dislocation to divert towards the hanging wall (to the left side). As a result, the foundation is not subjected to substantial deformation: bending moments do not exceed 600 kNm (with a "heavy" reinforcement ratio, the ultimate design capacity M_{ult} of the d = 1.0 m piles could reach 3000 kNm), but the pile group remains practically intact. Observe also that the pilecap is not subjected to any measurable displacement or rotation.

Moving the fault rupture at s = 7 m (i.e. in the free-field, the fault would have emerged 2 m to the right of the footwall edge of the pilecap), the response of the group dramatically worsens (Fig. 6b). Now, a rather distinct bifurcation of the dislocation takes place, leading to development of two separate ruptures: the first one, *R1*, is diverted by the first row of piles towards the hanging wall (left); the second, *R2*, outcrops between the two rows of piles. As a result, the front row of piles (left) is being "pulled" outwards (to the left) and downwards by the moving hanging wall, while the back row (right) cannot follow as it lies on the footwall. This imposed differential displacement of the two pile rows, in combination with the kinematic restraints of the pilecap, leads to development of rather large bending moments of the order of 1500 kNm. Furthermore, pilecap displacement and rotation is now discernible.

The distress of the pile group is largest for s = 8 m (Fig. 6c). In contrast to the previous case, the dislocation now just misses the tip of the front pile row. Paradoxically, this small "detail" worsens the response of the soil-foundation system to a rather large extent. While in the previous case (s = 7 m), the rupture experienced bifurcation and diffusion as it interacted with first pile row, now such stress-relieving phenomena cannot develop: the rupture is left "free" to develop to its full extent between the two pile rows. Hence, the two rows suffer the largest differential displacement, which leads to bending moments M of the order of 2800 kNm (i.e. M almost reaches M_{ult}) and measurable displacement and rotation of the pilecap. It would be interesting to think of this case in reality: while for an observer at the ground surface the rupture would appear to have missed the foundation, due to its non-vertical propagation path it would have intersected with the two pile rows inflicting substantial pile distress and rotation of the superstructure.

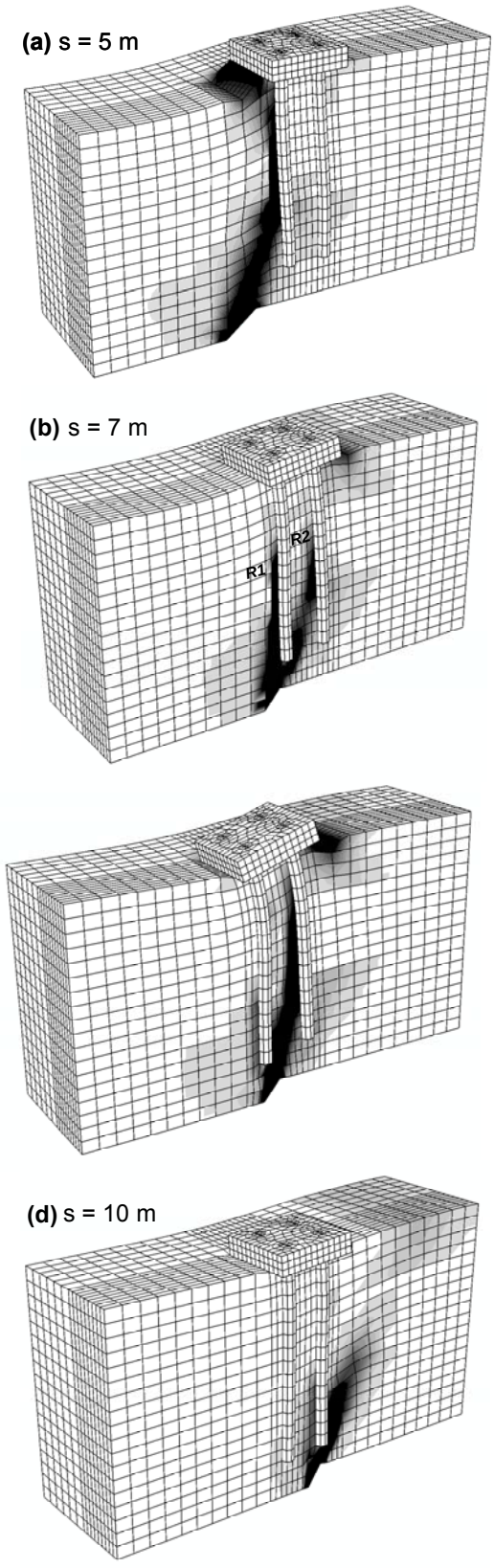

Fig. 6. FE deformed mesh with superimposed plastic strain contours for the 2 x 4 pile group, subjected to h = 0.05 m normal faulting (deformation scale factor = 40) : (a) s = 5 m, (b) s = 7 m, (c) s = 8 m, and (d) s = 10 m.

Moving the fault rupture to s = 10 m (Fig. 6d) leads to less stressing of the piles. Now, the propagating rupture plane intersects the tip of the back row of piles, undergoes substantial diffusion and limited local bifurcation. Both pile rows are lying on the hanging wall, being subjected to almost the same horizontal and vertical displacements. As a result, they are not subjected to substantial differential displacements, and consequently the tectonically-induced M does not exceed a mere 300 kNm. The rotation of the pilecap, which is directly related to the differential displacement between the pile rows, is insignificant. In stark contrast, since the whole pile group is moving along with the hanging wall, horizontal and vertical displacements at the pier base are substantial.

Fig. 7 summarizes the results, giving emphasis to the effect of the location s of fault outcropping to: (a) the horizontal Δx and vertical Δy displacement at the pier base, (b) the rotation θ at the pier base, (c) the maximum and minimum bending moments M of the piles, and (d) the maximum and minimum axial forces N of the piles. One would have expected that Δx and Δy are in general increasing with s : as the location of the rupture moves to the right, the pile group tends to be more on the hanging wall, being subjected to larger displacements. However, Δx and Δy at the pier base are also related to the rotation θ of the pilecap. The latter is directly related to the differential displacement between the two rows of piles, and is thus maximum for s = 8 m. As a result, Δy at the pier base is also largest for the same rupture location. On the other hand, Δx is not affected to the same extent by θ, being maximum for s = 10 m. Being the direct result of the differential displacement between the two pile rows, the stressing of the piles (exhibited through M and N) is also largest for s = 8 m (i.e. when the rupture outcrops exactly between the two rows).

In summary, it has been shown that a rather minor bedrock offset (h = 0.05 m in the case examined herein) is enough for typical end-bearing piles to reach their ultimate structural capacity, even in case of very "heavily" reinforced piles.

Performance of "large" 3 x 3 pile-group

This section deals with the "large" 3×3 pile group, which would be a reasonable solution for the 7-span viaduct. Since the response of end-bearing piles has already been shown to be rather problematic, we now focus on the response of floating piles (i.e. Layer 2 being the same with Layer 1). The soil is assumed to be the idealized dense or loose sand. The vertical superstructure load transmitted onto the pile group is assumed equal to 7000 kN, typical for the 7-span viaduct.

To illustrate the effect of soil resilience, we compare the response of the pile group in dense and loose sand. Fig. 8 depicts the evolution of M with the increase of imposed bedrock offset h for normal faulting at distance s = 11 m (representing the worst-case scenario). In dense sand, all piles are subjected to substantial bending, with the hanging wall

side piles (pile 1) being stressed the most and the footwall side piles (pile 3) the least. Soil resilience is clearly beneficial in terms of pile stressing : in loose sand the maximum M is a little more than merely one third of that of dense sand.

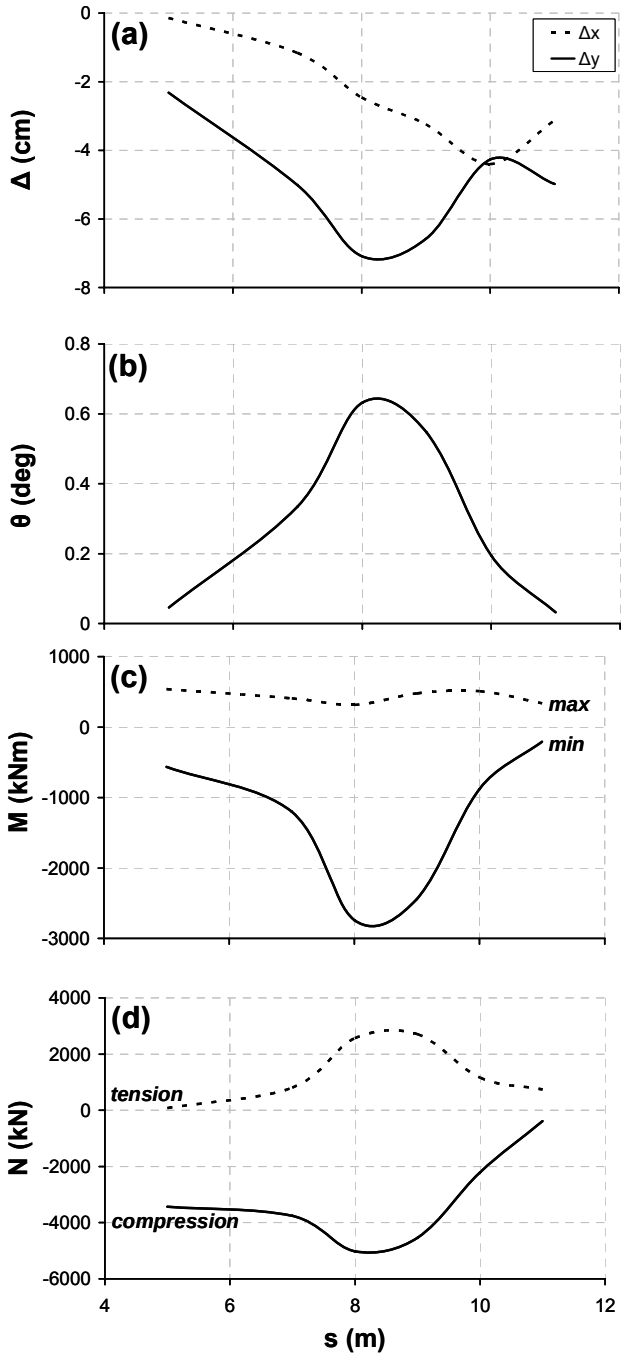

Fig. 7. Synopsis of analysis results for the 2 x 4 pile group, h = 0.05 m. Effect of the location s of fault outcropping to : (a) horizontal Δx and vertical displacement Δy at the pier base; (b) rotation θ at the pier base ; (c) maximum and minimum bending moment M of the piles ; and (d) maximum and minimum axial force N of the piles.

Naturally, such large bending moments would exceed the ultimate capacity, M_{ult}, of the d = 1.5 m piles: with a very "heavy" reinforcement ratio of the order of 4%, M_{ult} would be of the order of 8000 kNm. This means that in dense and stiff soil the hanging wall side piles (pile 1) would be the first to fail, at h = 0.35 m, followed by the medium row (pile 2), at h = 0.52 m, and finally the footwall side row (pile 3), at h = 1.61 m. In stark contrast, in loose sand only the first row (pile 1) would fail, and for substantially larger imposed deformation: h = 0.93 m. Note also that while at the early stages of deformation (h < 0.3 m) the stressing of the three pile rows is qualitatively similar to the case of dense sand (pile 1 is stressed the most; pile 3 the less), the increase of the imposed deformation leads to a mechanism change : the footwall side piles (3) experience more stressing than the medium row (2).

The demonstrated beneficial role of soil resilience is triple :

(a) In terms of *quasi-elastic behavior* : Before the soil surrounding the piles starts to yield, the decrease of soil stiffness leads to an increase of the relative pile stiffness, facilitating pile resistance to the imposed deformation ;

(b) In terms of *plastic behavior* : The decrease of soil strength (φ_p = 45° in dense sand ; φ_p = 32° in loose sand) speeds up soil failure at the pile-soil interface, allowing the piles to sustain larger imposed deformation before reaching structural failure. Stress relieving phenomena, such as fault rupture diversion and bifurcation, and diffusion of plastic deformation are also facilitated ; and

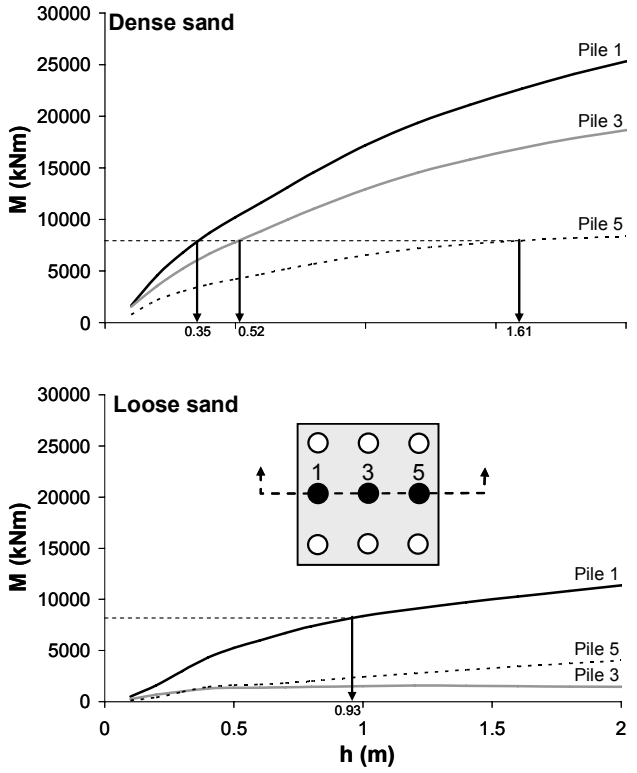

Fig. 8. The beneficial role of soil resilience for the "large" 3 x 3 pile group, subjected to normal faulting at s = 11 m : pile bending moments M with respect to bedrock offset h.

(c) In terms of *post failure behavior* : After the soil at the pile-soil interface has reached failure, the decrease of soil dilatancy ($\psi_p = 18^o$ in dense sand; $\psi_p = 3^o$ in loose sand) leads to a substantial decline of the rate of increase of pile stressing with the imposed deformation h. Observe in Figure 8 that while in dense sand the evolution of pile stressing with h exhibits a hardening-like behavior, in loose sand it resembles an elastic-perfectly plastic one.

All three reasons are also responsible for the superior performance of floating piles (this group) compared to end bearing piles (2×4 pile group) : while only 5 cm of bedrock offset were enough for all of the d = 1.0 m end-bearing piles to reach structural failure, in dense sand the first row of the d = 1.5 m piles can sustain 35 cm before reaching failure ; the other two rows have even larger safety margins (0.52 m and 1.61 m). Analyses (not shown herein) of the 3×3 pile group with Layer 2 being changed to the idealized rock-type material confirm this conclusion. In fact, due to the disproportional increase of pile stiffness compared to M_{ult} (increasing d from 1.0 m to 1.5 m leads to a 500% stiffness increase, compared to a 260% increase of M_{ult}), the d = 1.5 m piles have even smaller safety margins if they are of the end-bearing type.

Hinged pile-to-cap connection : a solution to the problem

In all cases examined, the largest pile bending moments occur at the connection with the pilecap. This location is therefore the first candidate for plastic hinging. Preventing such failure by introducing a-priori a hinged pile–to–cap connection is rather intuitive. Furthermore, dynamic analyses (strong ground shaking, not faulting related) of pile groups have shown that the type of pile-to-cap connection greatly influences the performance of the foundation, with the hinged connection leading to substantially less pile distress, at the cost of larger cap displacements and rotations [Tazoh et al., 2002; Gerolymos et al., 2008]. The idea of a devise that allows such a connection was introduced in Japan after the devastating 1995 Kobe earthquake. One such devise, designed and manufactured by Shimizu Co. & Kubota Co., is schematically illustrated in Fig. 9 [after Tazoh et al., 2002].

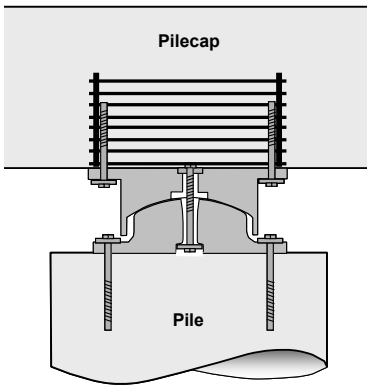

Fig. 9. Schematic of a hinged pile to pilecap connection [after Tazoh et al., 2002].

The cast-iron devise consists of a spherical table, a spherical lid, and a high-strength bolt at the center to allow transmission of tensile forces. Shear forces are transmitted through the high-friction contact surface (table–lid), while almost free rotation is allowed. The performance of this devise has been validated through real scale testing, and it has been applied in practice.

To qualitatively verify the effectiveness of such a solution for the problem investigated herein, the same pile groups were re-analyzed with hinged pile-to-cap connections. Typical results are shown in Fig. 10 for the case of the 3 x 3 pile group subjected to normal faulting at s = 9 m through idealized dense sand. Evidently, due to activation of the rotational degree of freedom the distress of all piles is drastically reduced. Even for h = 2 m (a rather large offset, typical of M > 7 earthquakes), M does not exceed 5000 kNm in any of the piles (Fig. 10a) — substantially lower than the largest possible ultimate capacity (M_{ult} = 8000 kNm) of the d = 1.5 m piles. As depicted in Fig. 10b, due to the hinged pile–to–cap connection the piles are now behaving like simply supported vertical beams, with M being maximum at almost the mid-height in the case of the hanging wall side row (pile 1), and at a shallower depth at the footwall side row (pile 5). The difference is clearly due to the more intense soil plastification at the front row of piles, which is more directly affected by the faulting-induced deformation.

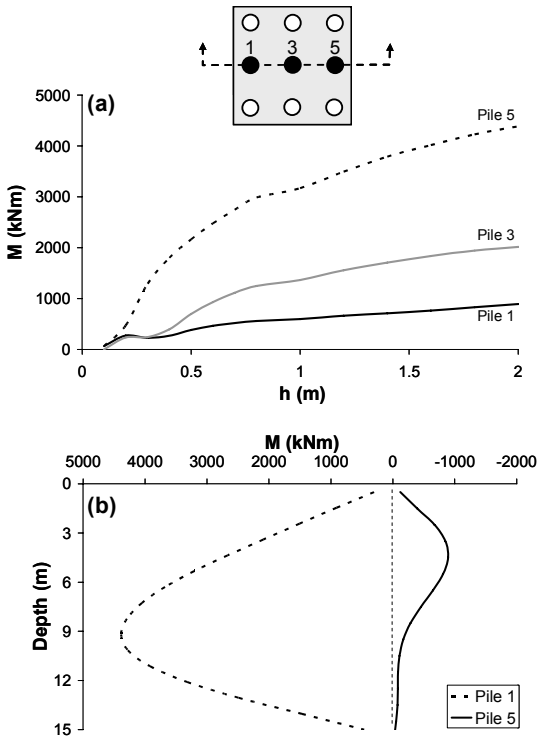

Fig. 10. The 3 x 3 pile group equipped with hinged pile–to–cap connections, subjected to normal faulting at s = 11 m through idealized dense sand : (a) evolution of pile bending moments M with the increase of imposed bedrock offset h ; (b) distribution of pile bending moments with depth.

CAISSONS

The seismic performance of caisson foundations is in general considered advantageous [e.g. Gerolymos & Gazetas, 2006], especially when subjected to large imposed deformation. The Kobe Ohashi and the Nishinomiya-Ko bridge in Kobe (Japan) partially owe their survival in the 1995 earthquake to their massive caisson foundations, which "intercepted" a substantial portion of the liquefaction–induced lateral spreading [Hanlong et al., 1997; Anastasopoulos et al., 2001]. In terms of faulting–induced deformation, the Banco Central de Nicaragua constitutes one of the earliest (and one of very few) such case histories. When the strike-slip fault rupture of the 1972 Ms 6.3 Managua earthquake "attempted" to cross the Bank, thanks to the existence of a rigid reinforced-concrete caisson (the Bank's underground vault), it was diverted leaving the building totally unscathed [Niccum et al., 1976].

In this section, we briefly discuss characteristic results of the parametric analysis that was conducted. We focus on the "large" 10 x 10 x 15 m caisson. Since caissons are commonly used as floating foundations, the soil is assumed homogenous, consisting of dense or loose sand. The caisson is assumed fully bonded to the bearing soil — a rather conservative idealization.

Fig. 11 illustrates the response of the caisson in idealized dense sand subjected to h = 2 m normal faulting at s = 1, 5, 9, and 13 m, in terms of FE deformed mesh with superimposed plastic strain. As depicted in Fig. 11a, for s = 1 m, the caisson diverts the dislocation towards the hanging wall (to the left), forming a distinct scarp at its left edge. Similarly to the case of the piled foundations, the caisson does not experience any measurable rotation or displacement.

Moving the rupture to the middle of the foundation, s = 5 m (Fig. 11b), leads to a more intense diversion of the rupture path: the fault now emerges vertically along the sidewall of the caisson. The latter experiences $\theta = 1^o$ and measurable vertical and horizontal displacements : Δy = 0.065 m and Δx = 0.28 m. Note also the formation of a secondary antithetic rupture zone, which starts propagating to the left of the main rupture at a dip angle of about 60^o. Reaching the surface, in combination with the main rupture (diverted to the left of the caisson), it generates a gravity graben : a feature purely related to the kinematic constraints imposed by the rigid caisson.

For s = 9 m (Fig. 11c), although the imposed deformation is diffused substantially, the caisson is subjected to rather intense rotation $\theta = 8^o$ and substantial vertical and horizontal displacements: Δy = 0.69 m and Δx = 2.19 m. Coulomb-type active conditions are likely to form at the back (footwall side) of the caisson. Finally, for s = 13 m (Fig.11d), the rupture path just intersects with the base corner of the caisson, being "defracted" towards the footwall (to the right), and finally emerging at the ground surface 8 m to the right of the footwall edge of the caisson: i.e., about 5 m to the right of its free-field outcrop location. The caisson essentially follows the the hanging wall, experiencing an appreciable rotation $\theta = 3^o$, combined with displacements $\Delta y \approx \Delta x \approx 1.65$ m.

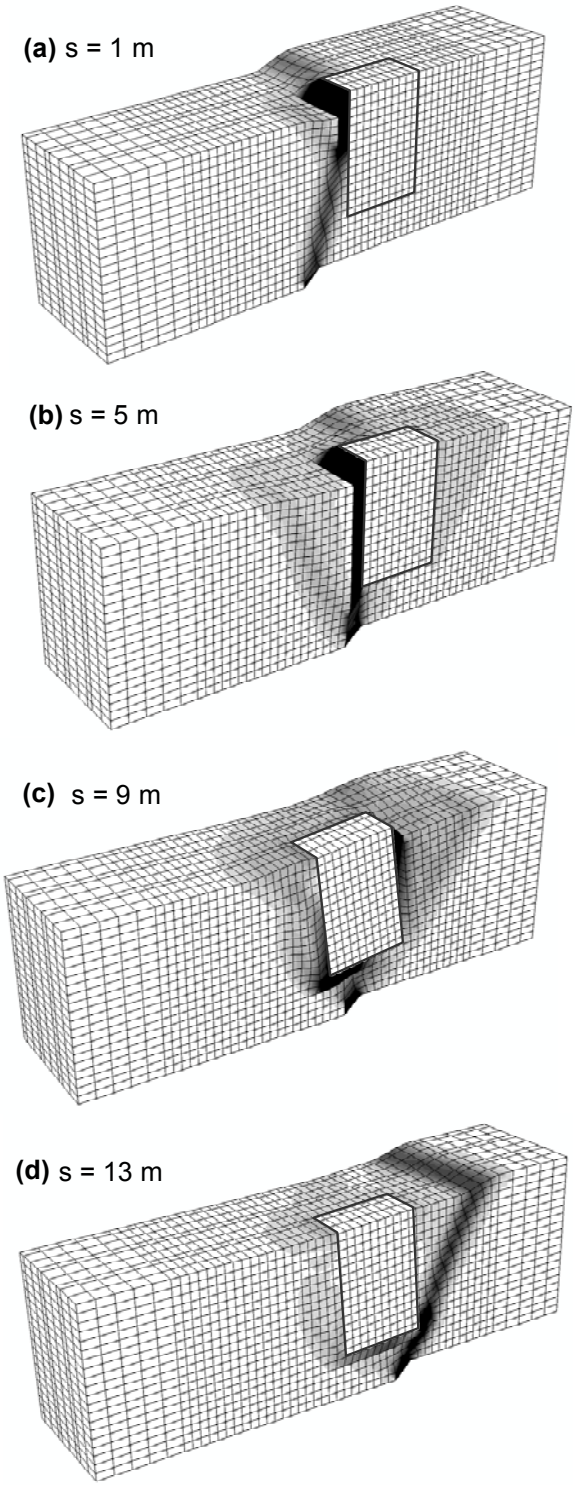

Fig. 11. FE deformed mesh with superimposed plastic strain contours for the caisson, subjected to h = 2 m normal faulting (deformation scale factor = 1) through idealized dense sand : (a) s = 1 m, (b) s = 5 m, (c) s = 9 m, and (d) s = 13 m.

TECTONIC STRESSING OF THE SUPERSTRUCTURE

Using the output of the first step (Δx, Δy, and θ at the base of the pier), in Step 2 (global level) we analyze the response of the detailed model of the superstructure. We focus the typical 7-span viaduct, which is of greater importance, and compare the two extreme cases : (a) continuous deck monolithically connected to piers, and (c) 7 simply supported spans on elastomeric (seismic isolation) bearings.

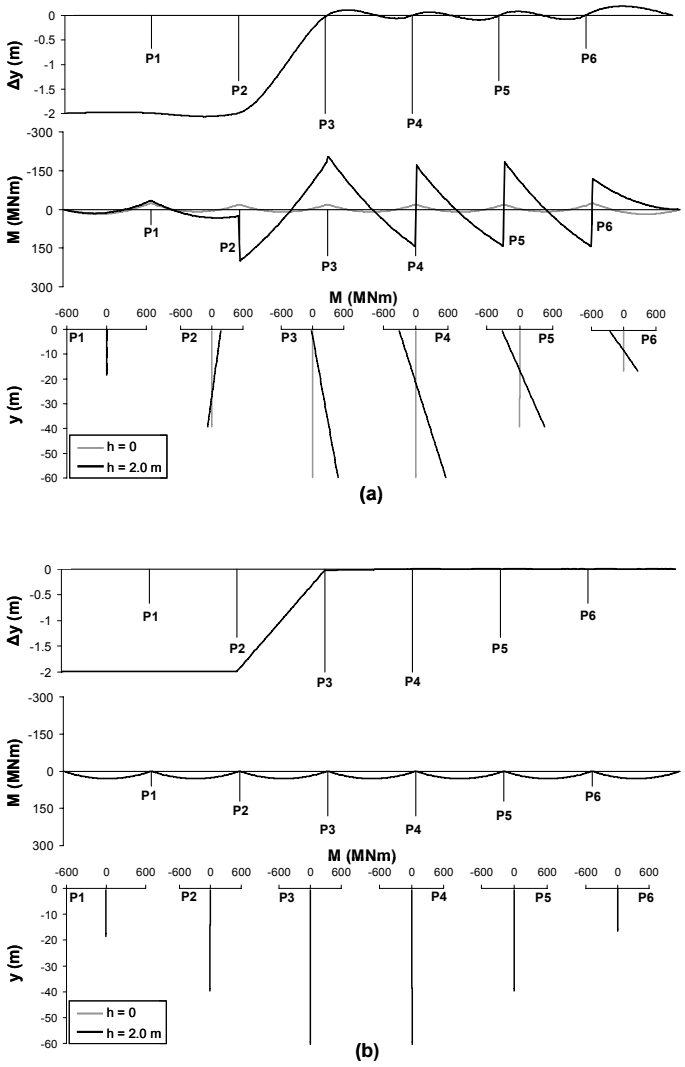

Fig. 13. The 7-span viaduct subjected to h = 2 m normal faulting at x = 150 m (i.e. at pier P3). Deck vertical displacement Δy and bending moments M of deck and piers for: (a) continuous deck monolithically con-nected to piers, and (b) 7 simply supported spans on elastomeric bearings.

The comparison is portrayed in Fig. 13 (h = 2 m normal faulting at x = 150 m, i.e. under pier P3), in terms of deck vertical displacements Δy and bending moments M along deck and piers. In the first case (continuous deck monolithically connected to piers), the imposed tectonic deformation generates large stressing (Fig. 13a). The tectonically-induced deck bending moments (black line) are an order of magnitude larger than their static (h = 0) values (in grey). Such stressing could not possibly be undertaken by any reasonable pre-stressed concrete box section — leading to failure. The stressing of the piers is also unacceptably intense.

The performance of the second alternative (7 simply supported spans on elastomeric bearings) is definitely favorable (Fig. 13b). In stark contrast to the statically indeterminate alternative, the imposed tectonic deformation does not cause any stressing of either the deck or the piers. The simply supported decks are only subject to rigid block type rotation and differential displacements. With adequate seating (to avoid deck falling), this alternative would survive even such a large tectonic deformation. Admittedly, the results shown herein refer to an extreme dislocation — deliberately to illuminate vividly the differences in response.

EXAMPLE APPLICATION OF THE METHODOLOGY

The methodology developed herein has already been applied in real life for the design against tectonic deformation of : (i) a 70 m 3–span road bridge in the island of Rhodes, (ii) a 40 m 3–span road bridge in Southern Greece, and (iii) a major 400 m 3–span arched rail bridge in Central Greece. The latter is presented to illustrate the applicability of our methodology.

The 400 m viaduct bridge crosses an active fault zone which is associated with the 1954 Sofades M ≈ 7 earthquake (Papastamatiou & Mouyaris, 1986). The length of the main rupture has been estimated to be of the order of 50 km with an average displacement of 1.8 m (Ambraseys & Jackson, 1990). With an estimated slip rate of 4 mm/year (Papadimitriou & Karakostas, 2003), the Sofades normal fault is the dominant seismotectonic feature of the broader area. Since the bridge is not directly crossing the main fault, but a secondary one, the conducted seismotectonic study concluded that the bridge should be designed for a bedrock offset h = 30 cm.

The initial bridge design was a typical viaduct with 10 simply supported pre-stressed concrete spans, with reinforced concrete piers, and founded through 3 x 3 pile groups. With the geotechnical profile mainly consisting of igneous periodite rock, initial FE analysis of the piled foundations showed that they could not possibly sustain the 30 cm design tectonic displacement. To satisfy the stringent design requirement that the bridge remains operational after the design seismic event (in order to avoid derailment, and to keep the rail network under operation), the largest post-earthquake longitudinal inclination should not exceed 20‰. The only way to achieve this was to increase the span length, by reducing the number of spans from 10 to 3.

As illustrated in Fig. 14, the improved design consists of three steel arch-type spans lying on seismic isolation spherical

sliding bearings. The latter were selected as the best compromise in terms of bridge performance to tectonic deformation and strong seismic shaking: they provide adequate restoring force *and* large permanent deformation limits. Shock transmission units are also installed between piers and decks to act as additional dampers in case of a strong earthquake. Such devices are activated only with large velocity: they do not react to pseudo-static loading, such as the tectonic deformation. Given the results of this research, rigid 10 x 22 x 15 m caissons were selected for foundation of the two hollow reinforced concrete (44 m and 47 m tall) piers.

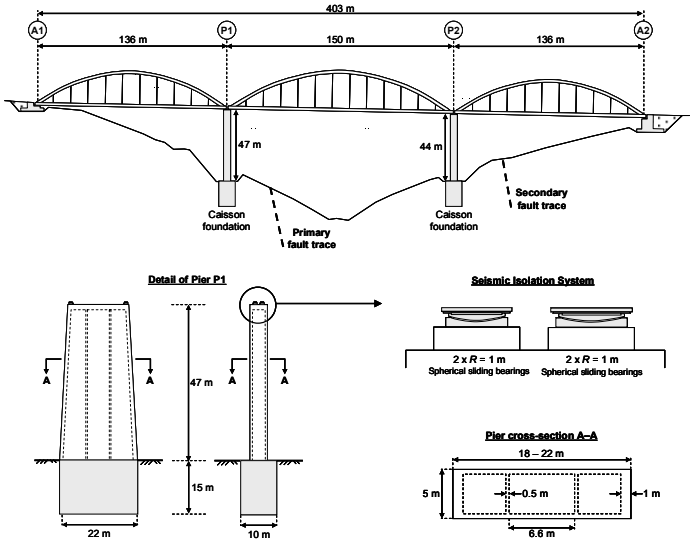

Fig. 14. Example application in Greece : the 3-span Domokos rail bridge, designed for h = 30 cm of normal bedrock offset. The initial bridge design (10 simply supported spans founded through 3 x 3 pile groups) was modified to cope with the design tectonic deformations.

With the methodology presented herein we analyzed the bridge for the design fault offset. Following the concept of Fig. 2, we first analyze the response of a single bridge pier (*Step 1*). Since the decks are seismically isolated, the lateral spring K_x was estimated on the basis of an equivalent tangent stiffness of the spherical sliding bearings; K_θ was assumed to be zero. Although the fault trace is clearly mapped, bearing in mind that the exact location of a fault rupture cannot be predicted accurately (e.g. Faccioli *et al*., 2008), the location of the fault rupture was parametrically investigated, both at the *local* (pier) and at the *global* (bridge) level.

At the *local* (pier-foundation) level four scenarios were investigated with respect to the location of fault rupture location : s = 5, 9, 13, and 16 m. The results are summarized in Fig. 15. Note that the maximum rotation appears at the base of the pier for s = 13 m, while the maximum vertical and horizontal displacements are observed for s = 16 m. Since the relative effect of Δx, Δy, and θ on the various components of the bridge superstructure (decks, piers, seismic isolation bearings, joints, etc) cannot be predicted with certainty, two *local* fault rupture scenarios are used in the *global* analysis of the bridge :

- Scenario "a" (fault rupture at s = 13 m) : Δx = 18.7 cm, Δy = 26.3 cm, and θ = 0.11 deg ;
- Scenario "b" (fault rupture at s = 16 m) : Δx = 17.7 cm, Δy = 17.1 cm, and θ = 0.24 deg.

Based on the results of the *local* level FR–SFSI analysis, seven different tectonic loading combinations as illustrated schematically in Fig. 16 are considered for the *global* level analysis of the superstructure. These combinations were then used to analyze the response of the bridge superstructure (*Step 2*). The seismic isolation devises, the seating of the decks, and the capacity of the joints were designed on the basis of the results of this analysis.

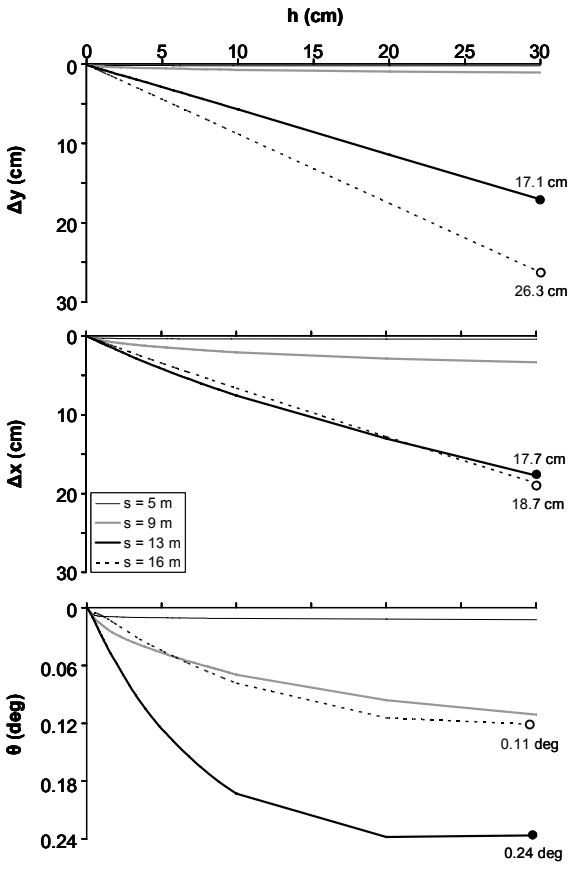

Fig. 19. Synopsis of analysis results for the 10 x 22 x 15 caisson : Evolution with bedrock offset h of vertical Δy and horizontal Δx displacement, and rotation $\Delta\theta$ at the base of the pier for the four locations s of fault outcropping.

Fig. 15. Synopsis of analysis results : vertical Δy and horizontal displacement Δx, and rotation Δθ at the base of the pier for the four locations s of fault outcropping.

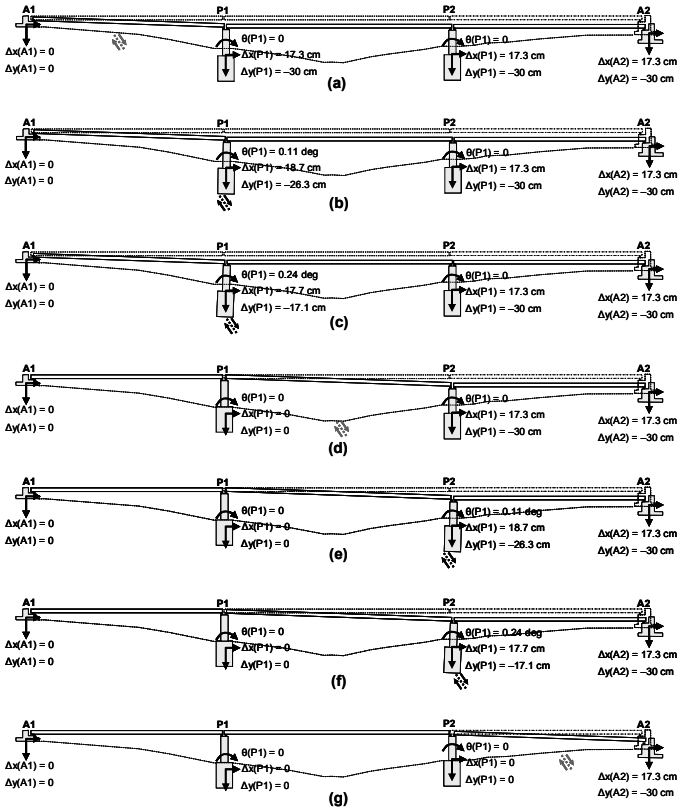

Fig. 16. The seven tectonic loading combinations : (a) fault rupture between abutment A1 and pier P1 ; (b) fault rupture at P1, scenario a ; (c) fault rupture at P1, scenario b ; (d) fault rupture between P1 and P2 ; (e) fault rupture at P2, scenario a ; (f) fault rupture at P2, scenario b ; and (g) fault rupture between P2 and A2.

CONCLUSIONS

This paper has presented a general methodology for the design of bridges against large tectonic deformation. The problem is decoupled in two analysis steps : the first (local level) dealing with the response of a single bridge pier subjected to fault rupture deformation; the second (global level) dealing with the detailed model of the superstructure. At the local level emphasis is given to fault rupture soil-foundation-structure interaction (FR-SFSI), with the superstructure modeled in a simplified manner to capture its kinematic constraints. The output of this local level analysis is treated as the input for the global analysis.

The main conclusions are as follows :

1. The design of bridges against tectonic deformation is quite feasible with proper design. The method of analysis presented herein may form the basis for future Code provisions and requirements on the subject.

2. In all cases investigated herein, the rupture path is strongly affected by the presence of the foundation. The emerging fault rupture is not only diverted, but is also subject to bifurcation and diffusion.

3. Piled foundations are in general quite vulnerable to faulting-induced deformation. End bearing piles cannot sustain even moderate bedrock offsets. Floating piles show better performance, which depends on soil resilience. The latter is in general beneficial in terms of pile stressing, but not necessarily for the inflicted displacements and rotation at the base of the pier. A hinged pile–to–cap connection may provide substantial stress relief, allowing a floating piled foundation to sustain larger imposed fault offsets, even of the order of a meter.

4. Rigid massive caisson foundations are clearly advantageous. The faulting-induced deformation will force the caisson to move and rotate as a rigid body, resulting in vertical and horizontal displacement and rotation at the pier base.

5. The location of fault outcropping plays a major role. For both piled and caisson foundations, displacements and rotation at pier base are not maximum for the same location of fault outcrop. Since the exact fault location would never be known precisely a-priori, its location relative to the foundation has to be parametrically investigated in design.

6. Continuous, statically indeterminate, superstructure systems are in general disadvantageous (the deck is forced to follow the imposed differential displacements). Statically determinate systems (such as multiple separate simply supported decks), allowing relative displacement and rotation without stressing are quite favourable.

7. In all cases, special care should be taken to avoid fall of the deck due to excessive relative displacements. Ample seating and adequate restraining devices, such as stoppers, are a necessity.

ACKNOWLEDGEMENT

This work was funded by OSE (the Greek Railway Organization), as part of the research project “Railway Bridges on Active Seismic Faults”.

REFERENCES

Anastasopoulos I., Gerolymos N., Gazetas G. (2001), Possible collapse reasons of an access span of the Nishinomiya-ko bridge : Kobe 1995, *Proceedings of the 4th Hellenic Conference on Geotechnical Engineering*, Athens, Vol. 2, pp. 83–90 (in Greek).

Anastasopoulos I., & Gazetas G. (2007a), Foundation-Structure Systems over a Rupturing Normal Fault : Part I. Observations after the Kocaeli 1999 Earthquake, *Bulletin of Earthquake Engineering*, 5 (3), pp. 253–275.

Anastasopoulos I., & Gazetas G. (2007b), Behaviour of Structure–Foundation Systems over a Rupturing Normal Fault : Part II. Analysis of the Kocaeli Case Histories, *Bulletin of Earthquake Engineering*, 5 (3), pp. 277–301.

Anastasopoulos I., Gazetas G., Bransby M.F., Davies M.C.R., and El Nahas A. (2007), Fault Rupture Propagation through Sand : Finite Element Analysis and Validation through Centrifuge Experiments, *Journal of Geotechnical and Geoenvironmental Engineering*, ASCE, 133 (8), pp. 943–958.

Anastasopoulos I., Gazetas G., Bransby M.F., Davies M.C.R., and El Nahas A. (2009), Normal Fault Rupture Interaction with Strip Foundations, *Journal of Geotechnical and Geoenvironmental Engineering*, ASCE, 135(3), pp. 359–370.

Berrill, J.B. (1983), Two-dimensional analysis of the effect of fault rupture on buildings with shallow foundations, *Soil Dynamics and Earthquake Engineering*, 2 (3), pp. 156-160.

Bransby, M.F., Davies, M.C.R., and El Nahas, A. (2008a), Centrifuge modelling of normal fault-foundation interaction, *Bulletin of Earthquake Engineering*, Special Issue : Integrated approach to fault rupture- and soil-foundation interaction, 6(4), pp. 585-605.

Bransby, M.F., Davies, M.C.R., and El Nahas, A. (2008a), Centrifuge modelling of reverse fault-foundation interaction, *Bulletin of Earthquake Engineering*, Special Issue : Integrated approach to fault rupture- and soil-foundation interaction, 6(4), pp. 607-628.

Bray, J.D. (1990), *The effects of tectonic movements on stresses and deformations in earth embankments*, Ph.D. Dissertation, University of California, Berkeley.

Bray, J.D., Seed, R.B., Cluff, L.S., and Seed, H.B. (1994a), Earthquake Fault Rupture Propagation through Soil, *Journal of Geotechnical Engineering*, ASCE, 120 (3), pp. 543–561.

Bray, J.D., Seed, R.B., and Seed, H.B. (1994b), Analysis of Earthquake Fault Rupture Propagation through Cohesive Soil, *Journal of Geotechnical Engineering*, ASCE, 120 (3), pp. 562-580.

Bray, J.D. (2001), Developing Mitigation Measures for the Hazards Associated with Earthquake Surface Fault Rupture, *Workshop on Seismic Fault-Induced Failures – Possible Remedies for Damage to Urban Facilities*, University of Tokyo Press, pp. 55-79.

Brune, J.N., and Allen, C.R. (1967), A low-stress-drop, low magnitude earthquake with surface faulting. The Imperial, California, Earthquake of March 4, 1966, *Bulletin of the Seismological Society of America*, 57, pp. 501-514.

Cole, D.A. Jr., and Lade, P.V. (1984), Influence Zones in Alluvium Over Dip-Slip Faults, *Journal of Geotechnical Engineering*, ASCE, 110 (5), pp. 599-615.

Duncan, J.M., and Lefebvre, G., (1973), Earth Pressure on Structures Due to Fault Movement, Journal of *Soil Mechanics and Foundation Engineering*, ASCE, Vol. 99, pp. 1153–1163.

Erdik M., (2001), Report on 1999 Kocaeli and Düzce (Turkey) Earthquakes, *Structural Control for Civil and Infrastructure Engineering*, Ed. by, F. Casciati, G. Magonette, World Scientific.

Faccioli, E., Anastasopoulos, I., Callerio, A., and Gazetas, G. (2008), Case histories of fault–foundation interaction, *Bulletin of Earthquake Engineering*, Special Issue : Integrated approach to fault rupture- and soil-foundation interaction, 6(4), pp. 557–583.

Gerolymos N., and Gazetas G. (2006a), Winkler model for lateral response of rigid caisson foundations in linear soil, *Soil Dynamics and Earthquake Engineering*, Vol. 26, No. 5, pp. 347–361.

Gerolymos N., and Gazetas G. (2006b), Development of Winkler model for static and dynamic response of caisson foundations with soil and interface nonlinearities, *Soil Dynamics and Earthquake Engineering*, Vol. 26, No. 5, pp. 363–376.

Gerolymos N., Giannakou A., Anastasopoulos I., and Gazetas G. (2008), Evidence of Beneficial Role of Inclined Piles : Observations and Numerical Results, *Bulletin of Earthquake Engineering*, Special Issue : Integrated approach to fault rupture- and soil-foundation interaction, 6(4), pp. 705–722.

Hanlong L., Susamu I., Ichii K. (1997), *Evaluation of deformation to the pneumatic caisson foundations of the Kobe Ohashi bridge*, Report of the Port and Harbor Research Institute, Japan.

Hwang, H.Y. (2000), *Taiwan Chi-Chi Earthquake 9.21.99. Bird's eye view of Cher-Lung-Pu Fault*, Flying Tiger Cultural Publ., Taipei, Taiwan, pp. 150.

Kawashima, K. (2001), Damage of Bridges Resulting from Fault Rupture in The 1999 Kocaeli and Duzce, Turkey Earthquakes and The 1999 Chi-Chi, Taiwan Earthquake, *Workshop on Seismic Fault-Induced Failures–Possible Remedies for Damage to Urban Facilities*, University of Tokyo Press, pp. 171-190.

Niccum, M.R., Cluff, L.S., Chamoro, F., and Wylie, L. (1976), Banco Central de Nicaragua : A case history of a high-rise building that survived surface fault rupture, in Humphrey, C.B., ed., *Engineering Geology and Soils Engineering*

Symposium, No. 14, Idaho Transportation Department, Division of Highways, pp. 133–144.

Pamuk, A., Kalkanb, E., Linga, H.I. (2005), Structural and geotechnical impacts of surface rupture on highway structures during recent earthquakes in Turkey, *Soil Dynamics and Earthquake Engineering*, Vol. 25, pp. 581–589.

Slemmons, D.B. (1957), Geological Effects of the Dixie Valley-Fairview Peak, Nevada, Earthquakes of December 16, 1954, *Bul. of the Seism. Soc. of America*, 47 (4), pp. 353–375.

Taylor, C.L., Cline, K.M. Page, W.D., and Schwartz, D.P. (1985), The Borah Peak, Idaho earthquake of October 28, 1983 – Surface Faulting and Other Phenomena, *Earthquake Spectra*, 2 (1), pp. 23–49.

Tazoh T., Ohtsuki A., Aoki T., Mano H., Isoda K., Iwamoto T., Arakawa T., Ishihara T., and Ookawa M. (2002), A new pile-head device for decreasing construction costs and increasing the seismic performance of pile foundations, and its application to structures, *Proc. 12th European Conference on Earthquake Engineering*, Elsevier Science Ltd. Paper No. 720.

Ulusay, R., Aydan, O., Hamada, M. (2002), The behaviour of structures built on active fault zones: Examples from the recent earthquakes of Turkey, *Structural Engineering & Earthquake Engineering*, JSCE, 19 (2), pp. 149–167.

Youd, T. L. (1989), Ground Failure Damage to Buildings During Earthquakes, *Foundation Engineering—Current Principles and Practices*, Vol. 1, pp. 758–770. New York: ASCE.

Youd, T. L., Bardet, J-P, and Bray, J.D. (2000), Kocaeli, Turkey, Earthquake of August 17, 1999 Reconnaissance Report, *Earthquake Spectra*, Suppl. A to Vol. 16, pp. 456.